Spatial–temporal variability in solar radiation during spring snowmelt

S. Pohl, P. Marsh* and A. Pietroniro

National Water Research Institute, 11 Innovation Boulevard, Saskatoon, SK, S7N 3H5, Canada.
Corresponding author. E-mail: *philip.marsh@ec.gc.ca*

Received 9 August 2004; accepted in revised form 11 February 2005

Abstract Much of the spring landscape of arctic regions is dominated by a patchy snow cover with implications for both spring melt runoff and atmospheric fluxes. In addition to a variable end-of-winter snowpack, spatial differences in snowmelt energy terms play an important role in the development of this patchy snow cover. This paper focuses specifically on the influence of solar radiation on snowmelt by using a model to simulate the small-scale variability of solar radiation incident on the ground surface due to topographic influences over a small arctic catchment. The model only requires a digital elevation model (DEM) and measured global radiation.

Despite the relatively low relief (average slope 3°) of the study area, the results showed solar radiation differences of up to 10% of the area-wide mean over the melt period. This would result in differences in snowmelt amounts of up to 50 mm, a value similar in magnitude to the overall mean end-of-winter snow water equivalent in the study region. An analysis of the effects of changing model scale showed that the simulated variability decreased substantially for larger grid sizes.

The results show that the small-scale variability of solar radiation contributes greatly to the mosaic patterns in melting snow covers of arctic regions, affects the timing and amount of meltwater release and influences the surface energy balance of these areas considerably.

Keywords Small-scale spatial variability; snowmelt; solar radiation

Introduction

Snowmelt and subsequent meltwater runoff play an important role in the hydrology of many northern basins. Furthermore, the decaying snow cover plays a crucial role in land–surface atmosphere interactions affecting surface albedo and turbulent fluxes of sensible and latent heat (Marsh and Pomeroy 1996). End-of-winter snow covers in arctic basins are often characterized by a high spatial variability due to redistribution of snow during frequent blowing snow events over the winter (Pomeroy *et al.* 1997). Recent studies have demonstrated that rate and magnitude of snowmelt is controlled by complex interactions between a variable snow water equivalent (SWE) and variable energy fluxes. The result of this heterogeneity is the quick development of a patchy snow cover, which further enhances spatial differences in melt rates through local scale advection (Marsh *et al.* 1997; Neumann and Marsh 1998).

Studies have shown that energy fluxes controlling snowmelt like radiation, turbulent fluxes of sensible and latent heat, and ground heat are typically not uniform (i.e. Hinzman *et al.* 1992; Marks *et al.* 1999). Amongst these fluxes solar radiation is usually the dominant term of the snowmelt energy balance, especially in open environments like arctic tundra basins (Male and Granger 1981; Ohmura 1982). Simulations of solar radiation generally first calculate clear-sky radiation values for horizontal surfaces and subsequently modify these for cloud cover and topographic effects. As solar radiation passes through the atmosphere, it is attenuated due to absorption and scattering processes, with the amount of radiation not scattered or absorbed being termed direct radiation (Iqbal 1983). Scattered radiation is

doi: 10.2166/nh.2005.026

Nordic Hydrology **Vol 37 No 1 pp 1–19** © Environment Canada 2006

eventually directed back towards space or to the Earth's surface as diffuse radiation. The total amount of solar radiation incident on the Earth's surface (global radiation) consists therefore of the sum of direct radiation from the solar beam and diffuse solar radiation scattered in the direction of the monitoring point (Tian *et al.* 2001).

The amount of radiation incident on any point of the Earth's surface is modified by the topography. These effects can be addressed by determining the slope and aspect of individual grid cells and the presence of projected shadows in a DEM in relation to the incoming solar beam at every time step. The relationship between slope surface angle and solar altitude and azimuth angles controls the amount of direct radiation incident on a particular location.

To be useful for snowmelt runoff simulations and other applications, any model of solar radiation will have to be extended for cloudy sky conditions. Cloud cover reduces the amount of direct radiation reaching the Earth's surface while increasing the relative contribution of diffuse radiation to overall global radiation values. Most methods of estimating radiation under such conditions use a cloudiness index to account for differing cloud conditions (Dozier 1978). Obtaining the amount of diffuse radiation is often difficult. Some models require information on atmospheric conditions from soundings or atmospheric models (Dozier 1978; Munro and Young 1982; Dubayah *et al.* 1990), while other models (including the one used in this study) quantify diffuse irradiation from algorithms that only require *in situ* pyranometer data on global radiation (Ranzi and Rosso 1991, 1995; Dubayah and van Katwijk 1992). Such a simple model structure is crucial for arctic studies due to the paucity of atmospheric data in that region.

Diffuse radiation is anisotropic, with more diffuse radiation coming from parts of the sky closest to the Sun. However, the modelling of this anisotropy is complex and, as a result, many models assume isotropic diffuse radiation (Dubayah 1994). The amount of diffuse solar radiation incident on a grid cell is therefore assumed to be only dependent on its elevation and on the portion of sky actually visible to it, termed the sky view factor (Obled and Harder 1978; Munro and Young 1982). Adjacent terrain features may also have significant effects on the incident solar radiation of a point. A number of grid cells within a model domain might lie in the shadow of such features. A slope can also be "self shadowing" if it is facing away from the Sun and its gradient is steeper than the solar elevation angle (Dubayah and Rich 1995). Shadowed grid cells are significantly less irradiated as they do not receive any direct radiation. On the other hand, a grid cell may receive additional radiation reflected from adjacent terrain features.

The topographic effect on solar radiation in mountainous or rugged terrain has been clearly demonstrated in a number of studies, including Dozier (1978, 1980), Munro and Young (1982), Dubayah (1994), Dubayah and van Katwijk (1992), and Dana *et al.* (1998). However, very few studies have considered the variability of solar radiation in low relief areas (Dubayah *et al.* 1990) and its effect on snowmelt in these areas (Hinzman *et al.* 1992). Despite these studies, the sub-grid variability of solar radiation has so far been omitted in most land–surface components of atmospheric models, regional climate models, general circulation models and numerical weather prediction models (Slater *et al.* 2001), as well as some large scale hydrological models like WATCLASS or SRM (Brubaker *et al.* 1996; Soulis *et al.* 2000).

It is the objective of this paper to use a solar radiation model to simulate the small-scale variabilities in incident solar radiation as a result of topography and to assess their implications for snowmelt processes. The results will illustrate the magnitude of the variability present even in the gentle topography typical of many arctic catchments and quantify its effect on snowmelt processes. It will also address the effect of model scale on simulated variability of solar radiation and melt rates.

This paper is the first in a series aimed at studying the small scale spatial variability in the energy fluxes controlling snowmelt in a low relief arctic tundra basin. It will focus on an arctic study site, since aircraft measurements have shown high variabilities in surface energy fluxes of arctic spring landscapes compared to other environments such as grasslands, agricultural lands, and temperate forests (Brown-Mitic *et al.* 2001). Furthermore, due to its simplicity the presented model is well suited for data-sparse regions, such as the arctic. However, the overall conclusions as well as the techniques developed and applied in this paper are applicable to a wide range of snow covered open environments.

Study area

The study was conducted in the National Water Research Institute research basin of Trail Valley Creek (TVC) in the Northwest Territories during the period from mid-April to early June 1999 as part of the Mackenzie GEWEX Study/Canadian GEWEX Enhanced Study (MAGS/CAGES) program. TVC is located 55 km northeast of Inuvik at approximately 68° 45′ N, 133° 30′ W. The area is characterized by gently rolling hills with some deeply incised river valleys. Elevation ranges from 9–187 m a.s.l. (Figure 1) with an average elevation of 99 m a.s.l. Mean slope is 3° with the maximum gradient reaching 33°. Figure 1 shows a shaded relief map of the study area. The illumination angle is at an azimuth of 315° and at an elevation of 30°. The region lies at the northern edge of the forest–tundra transition zone, with tundra vegetation dominating much of the upland areas and some shrub tundra and sparse black spruce (*Picea mariana*) forest on moister hill slopes and in the valley bottoms (Neumann and Marsh 1998).

Studies have shown that the end-of-winter snow cover in TVC is highly variable due to redistribution of snow during blowing snow events (Essery *et al.* 1999; Pomeroy *et al.* 1997). Pomeroy *et al.* (1997) show SWE varying from 54–419% of measured snow fall for the end-of-winter snowpack of 1993. Snowmelt in the region usually occurs during May and June. In the spring of 1999 snowmelt started around 5 May as daytime temperature rose above the freezing point and lasted until about 10 June.

Two permanent observing stations recording meteorological conditions, including incoming global and diffuse (only at one of the stations) short wave radiation are situated in the basin. In order to carry out the radiation modelling, a DEM showing an area of 18 × 15 km^2 around TVC was used, with the complete DEM consisting of 168 750 grid cells

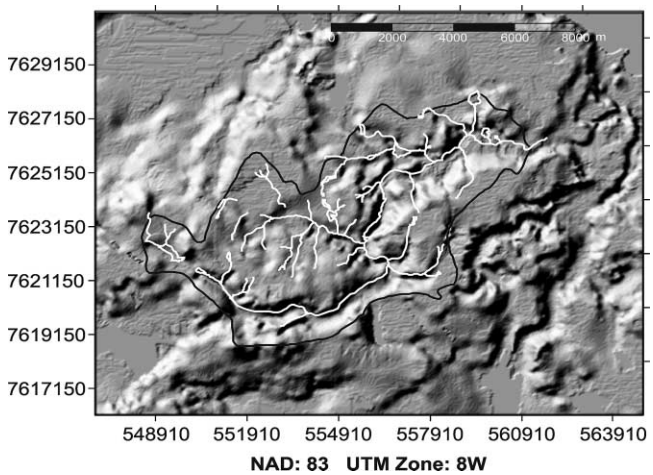

Figure 1 Shaded relief map of TVC and surrounding areas (illumination angle is located at azimuth of 315° and at elevation of 30°). Overall elevations range from 9–187 m a.s.l

with a resolution of 40 m. This DEM was obtained by digitizing 1:50 000 National Topographic Survey maps.

Methods

The model simulating topographical effects on incident solar radiation was run for each hour from sunrise to sunset for 33 d from 5 May to 6 June 1999 and subsequently for the same time period in 1998 and 2001. The Sun is above the horizon for 18 h from 5–15 May, 20 h until 24 May, 22 h until 27 May and 24 h after that date.

Description of the radiation model

The radiation model used in this paper largely follows an approach outlined by Ranzi and Rosso (1991) and was implemented in the GIS package PCI. The first step in the modelling process is the calculation of solar elevation, zenith ($s(t)$) and azimuth angles from geographical location, date and solar time. These angles are used to determine the theoretical amount of solar radiation reaching a horizontal plane at the Earth's surface under clear sky conditions followed by a consideration of topographic effects and cloudy sky conditions.

Clear sky horizontal plane radiation. Direct clear sky radiation R_c is computed by

$$R_c = I_o \exp(-T/\cos s(t))\cos s(t) \quad (1)$$

where I_o is the extraterrestrial irradiance and T is the optical depth of the atmosphere. I_o can be calculated from

$$I_o = EI_{sc} \quad (2)$$

with I_{sc} being the solar constant (1367 W/m^2) and E the eccentricity correction accounting for the change in distance between Earth and Sun during the year (Iqbal 1983). The optical depth T in Equation (1) accounts for atmospheric absorption and scattering processes. Since the number of absorbers and scatterers change with height, T was adjusted for elevation differences in the model area. This, however, lead to only minimal variations in T (within 1.5%) due to the low elevation range in the study area.
Clear sky diffuse radiation D_c is computed from

$$D_c = KI_o\cos s(t)\,[1 - \exp(-T/\cos s(t))] \quad (3)$$

where K is a dimensionless diffusion parameter. Due to the difficulties in measuring T and K with standard meteorological stations, values of 0.23 (at a reference elevation of 75 m) and 0.3, respectively, were determined as best fit parameters from regression analyses comparing model outputs with measured data on clear days. These values are very close to those reported in other studies (Dubayah *et al.* 1990; Ranzi and Rosso 1995).

Total clear sky incoming solar radiation G_c incident on a horizontal plane at the surface can then be calculated from

$$G_c = R_c + D_c \quad (4)$$

Cloudy sky horizontal plane radiation. Cloud cover, expressed as a cloudiness index d_i, is assessed by comparing the theoretical values of G_c (from Equation (4) for clear sky conditions) against observed incoming solar radiation G_o. A lower threshold for solar radiation penetrating a completely cloudy sky is set by multiplying G_c with a transmissivity coefficient T_{co}. Male and Granger (1981) suggested using a T_{co} of 0.22 for a 8/8 stratocumulus cloud cover. For G_o lower than this threshold, d_i reaches its maximum of 1 and radiation is considered to be completely diffuse. A linear relationship is formulated for all other cases so that

$$d_i = (G_c - G_o)/[(1 - t_{co}))G_c] \tag{5}$$

G_o is then partitioned into modelled direct R_m and diffuse D_m (Ranzi and Rosso 1991) from

$$D_m = (1 - d_i)D_c + d_i G_o \tag{6}$$

$$R_m = G_o - D_m \tag{7}$$

Topographic effects on surface radiation. The amount of incident solar radiation for a given grid cell of a DEM is affected by:

(a) whether the grid cell is shadowed by adjacent terrain or the slope itself, and
(b) by the slope and aspect of the grid cell in relation to the solar angles.

In the model, every grid cell is checked at each time step for shadowing effects with shadowed grid cells only receiving the modelled diffuse radiation D_m values, which vary slightly with elevation due to the varying T. The amount of direct solar radiation, which non-shadowed grid cells receive in addition to that, is determined from the slope and aspect of each grid cell and from respective solar angles using standard geometric calculations (Tian *et al.* 2001; Bloeschl *et al.* 1991). Slope and aspect of a given grid cell is determined from the elevation difference to its 8 nearest neighbours in the DEM. Other effects of adjacent terrain features on diffuse radiation (i.e. obstructed sky-view and reflected radiation) were not considered in this study due to the gentle topography of the study area.

Results

Model validation

Simulated values for hourly incoming clear-sky global radiation G_c were compared to measured values of G_o at two sites in TVC for several cloud-free days during the melt period. An average of the two sites was used to minimize instrumentation errors and to provide an area wide average. Topographically, both stations were situated on completely flat and open terrain. The modelled radiation differed from measured radiation by as much as $\pm 80\ \mathrm{W/m^2}$ (Figure 2), probably due to the occurrence of thin clouds and slight short term variations of T and K. Overall, model results correlated very well with measured data ($R = 0.98, R^2 = 0.95$). This good relationship is not unexpected since the modelled data was "forced" to fit clear-sky observed values through the parameters T in Equation (1) and K in Equation (3). However, it does indicate that this simple approach for estimating incoming clear-sky solar radiation is reasonable, and that large changes in T and K did not occur over the study period.

Model predictions of incoming hourly diffuse radiation (D_m) were checked against measured values for multiple days with a wide variety of cloud conditions. These values were not used in the model calibration. The model seemed to slightly overestimate D_m on cloud-free days, while slightly lower than observed values were apparent for cloudy days.

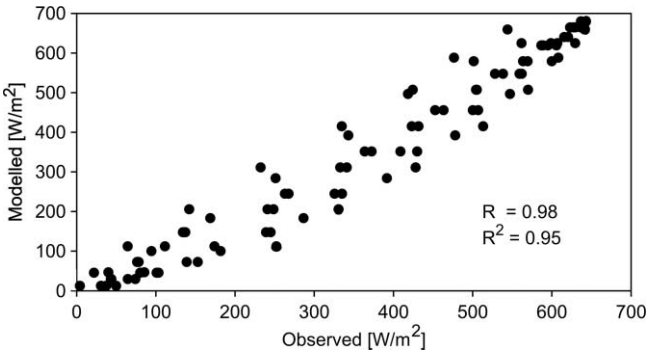

Figure 2 Hourly values of modelled (G_c) vs. observed incoming (G_o) clear-sky global radiation for 5 clear days (10, 13, 22, 27 May and 8 June) during the spring of 1999

Days with variable cloud conditions were predicted fairly well (Figure 3). The overall correlation for hourly values of D_m for 12 randomly selected days had an R of 0.93 ($R^2 = 0.86$) with a standard error of the estimate of 26.2 W/m^2 (Figure 4). This shows that the entire model simulation is working well, as values of diffuse irradiation under varying cloud conditions are often very difficult to simulate accurately (Dubayah and Rich 1995).

Spatial variability in radiation

Figure 5 shows maps of distributed hourly incident solar radiation for 27 May which was a clear day. In the early morning (Figure 5(a)) large shadowed areas can be seen to the west of ridges (see Figure 1), while peak radiation occurs on north-east facing slopes. By midday, south facing slopes receive maximum radiation inputs (Figure 5(b)) and only a very small fraction of the area is shadowed due to the high Sun angle and fairly low topography of the study region. Figure 5(c) shows afternoon conditions with increased radiation values on south-west to west facing slopes and shadows reappearing as the Sun elevation angle decreases. The respective distributions of incident solar radiation values are shown in Figure 6 along with the histograms of incident radiation for a fully cloudy day (31 May 1999).

The range of values is in excess of ± 100 W/m^2, with the modal class increasing from near 200 W/m^2 at 04:00 to 710 W/m^2 at 12:00 and then decreasing to 550 W/m^2 at 16:00. These values are very close to measured or modelled values of global radiation for horizontal surfaces, which is expected for all basins that are sufficiently large compared to the topographic variability. However, for smaller sub-basins with dominant slope directions, basin-wide average global radiation may be considerably different from that observed for a plane surface.

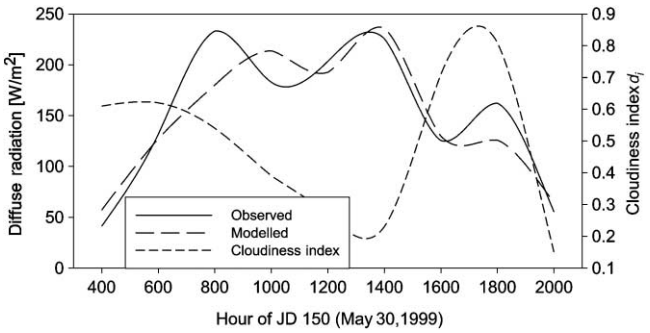

Figure 3 Modelled diffuse radiation (D_m) vs. observed diffuse radiation on 30 May 1999 including cloudiness index

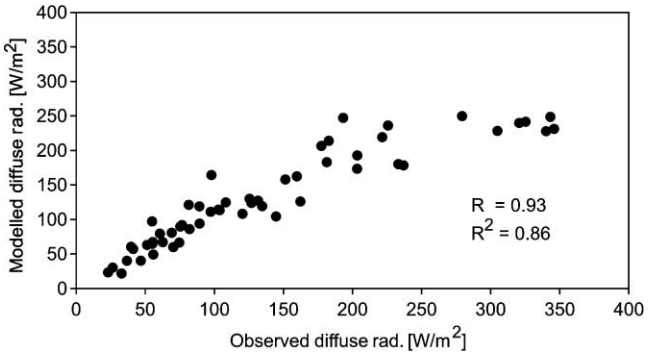

Figure 4 Hourly values of modelled diffuse radiation (D_m) vs. observed diffuse radiation for cloud conditions ranging from clear to fully cloud covered (12 d)

Table 1 shows examples for hourly model outputs, including mean values and variability over the model domain for five days with varying cloud conditions. 31 May was completely cloudy, 17 May was mostly overcast, 19 May had variable clouds with sunny periods in the afternoon, while 21 May and 27 May were clear and sunny. The results show that the variability within the model domain is dependent on the amount of cloud cover and on solar elevation angles. Topographic control is greatest on clear days, since much of the incident global radiation arrives as direct radiation, which is more sensitive to differences in slope and aspect. Increasing cloud cover resulted in much higher relative contributions of evenly distributed diffuse radiation to overall global radiation and therefore decreased variability. Similar trends were reported by Munro and Young (1982).

These results indicate that melt rates are dependent on cloud conditions. On cloudy days the overall contribution of solar radiation to snowmelt is generally lower but large areas of the basin will have fairly even melt rates. On clear days melt rates will vary greatly throughout the basin, potentially leading to a more variable meltwater release. Figure 7 shows the average incident solar radiation and the resulting melt rates (assuming an albedo of 0.7), for east, south, west and north facing slopes greater than 8° as well as for flat areas for a cloud-free day (27 May). Also shown is the (hypothetical) diffuse radiation that would be transferred evenly to the surface for a completely cloudy day ($d_i = 1.0$). This graph shows the importance of terrain for the timing and magnitude of melt.

As expected, south facing slopes show the highest average daily melt rates. Conversely, north facing slopes actually have the highest melt rates in the early morning and late evening hours due to the long daylight hours at this latitude. Furthermore, although west and east facing slopes have fairly similar accumulated daily solar irradiation values, their daily melt rates can be quite different. West facing slopes receive maximum solar radiation about 6 h later during the afternoon hours, coinciding with the highest daily air temperatures. Additionally, any night-time radiative energy loss of the snow cover has generally been erased by this time, often leading to much higher melt rates on west facing compared to east facing slopes (Hinzman *et al.* 1992).

Prior to the snow cover being isothermal, the energy differences evident in Figure 7 will lead to differences in the timing of snowpack ripening. Snow covers of basins that are frequently cloud covered during the early snowmelt period will ripen slower but more evenly across the basin, leading to a sharper meltwater runoff curve once runoff has been initiated. Mostly sunny conditions during early melt will cause considerable differences as to when different areas of the basin start to contribute to snowmelt runoff, resulting in an earlier but broader hydrograph.

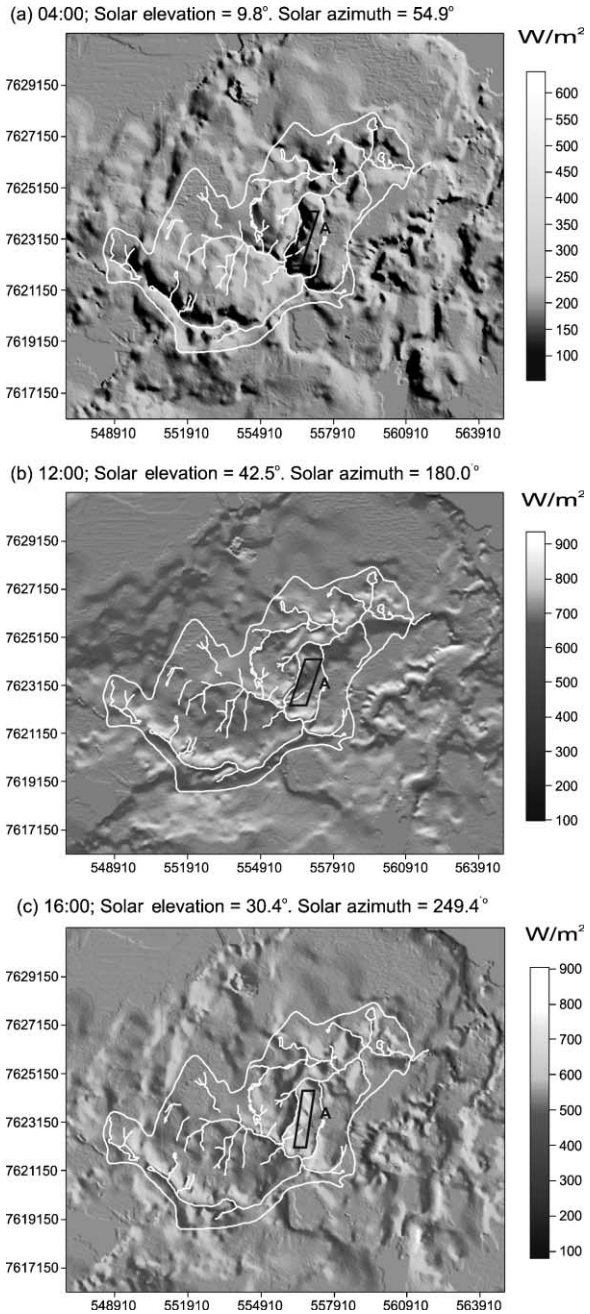

Figure 5 Modelled hourly incident global radiation in W/m^2 for 27 May 1999. (All times shown in solar time, Sky conditions clear throughout $d_i = 0$)

As mentioned earlier, the model was run for the same time period in 1998 and 2001. Figure 8 shows average hourly cloudiness indices over the three modelled spring melt periods. It becomes evident that there is a clear diurnal trend in the cloudiness which can be attributed mainly to the frequent development of night time inversions over melting snow covers (Martin and Lejeune 1998). The increased amount of clouds during the morning hours further enhances differences in melt rates between east and west facing slopes, as maximum solar irradiation on east facing slopes coincides with times of above average cloudiness,

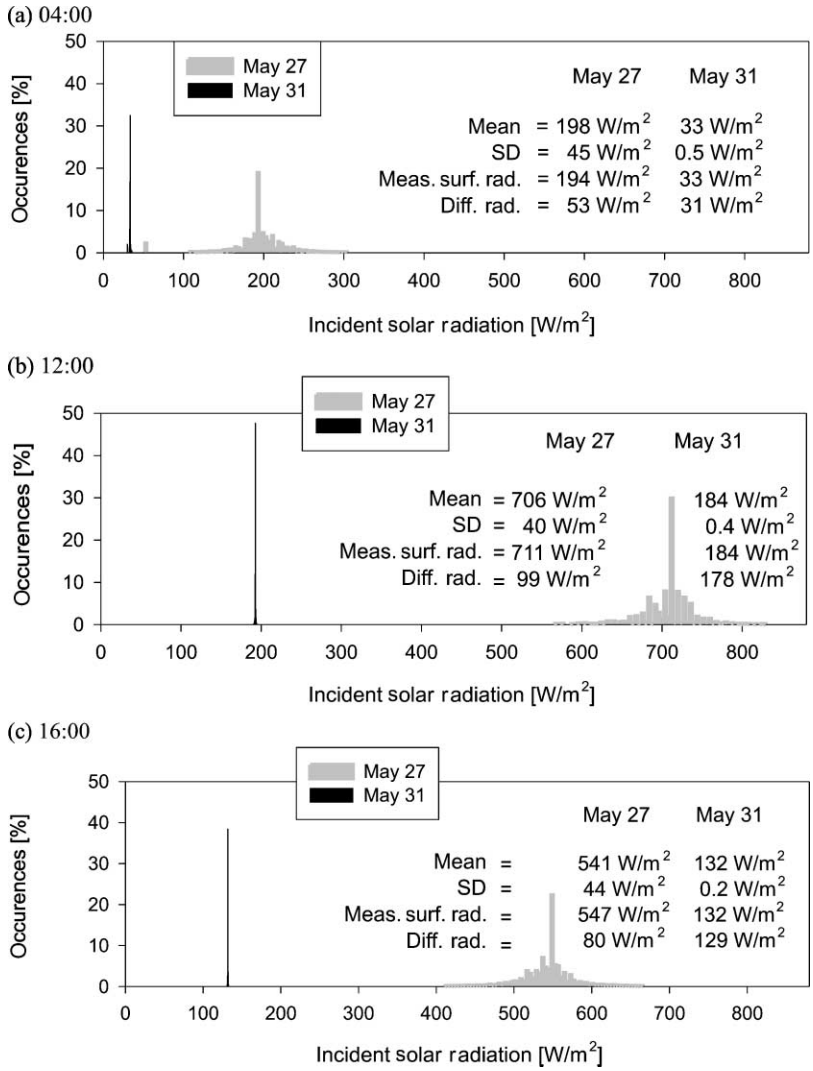

Figure 6 Histograms of hourly incident global solar radiation for 27 May 1999 and 31 May 1999. (All times shown in solar time. Sky conditions on 27 May clear throughout ($d_i = 0$), completely cloudy on 31 May ($d_i = 1.0$)

while west facing slopes receive maximum contributions of solar radiation during the less cloudy afternoon hours.

For all three years modelled, hourly maps of distributed incident solar radiation were added together to obtain cumulative values expressed in MJ/m^2. Table 2 shows the radiation statistics for three sub-periods as well as for the total study period of the three years. The difference in mean accumulated radiation between the years can be attributed to varying cloud conditions. Also shown are the relative contributions of diffuse radiation to overall incoming solar radiation. The amount of diffuse radiation received by the snow cover is crucial for snowmelt studies, as it provides an estimate of minimum melt rates due to solar radiation in perpetually shadowed areas on steep north facing slopes and in deeply incised river valleys.

Over the three model periods almost half of the solar radiation incident on the snow cover was diffuse. The highest relative diffuse contributions were observed, as expected, on completely cloudy days like 31 May 1999 (see Table 1), when 98% of incoming solar

Table 1 Hourly values of incident solar radiation, range, standard deviations (SD) and cloudiness index (d_i) for four days with different cloud conditions

Date	Hour	Mean (W/m^2)	Range (W/m^2)	SD (W/m^2)	SD (% of mean)	d_i
31 May	600	66	0.3	0.01	0.0	1
	900	128	1	0.04	0.0	1
	1200	184	2	0.36	0.2	1
	1500	150	6	0.21	0.1	0.98
	1800	80	1	0.06	0.1	0.98
17 May	600	102	17	1	0.9	0.75
	900	276	106	5	1.6	0.64
	1200	354	139	5	1.4	0.61
	1500	298	133	5	1.8	0.58
	1800	133	58	3	2.3	0.59
19 May	600	137	56	3	2.2	0.57
	900	358	219	9	2.6	0.44
	1200	489	334	12	2.4	0.36
	1500	413	324	13	3.1	0.32
	1800	177	142	8	4.3	0.36
21 May	600	327	534	29	8.9	0
	900	561	686	28	5.1	0
	1200	640	646	23	3.6	0.08
	1500	533	614	24	4.4	0.03
	1800	266	426	23	8.5	0
27 May	400	198	587	45	22.7	0
	800	515	752	43	8.4	0
	1200	706	838	40	5.7	0
	1600	541	825	44	8.2	0
	2000	155	451	35	22.6	0

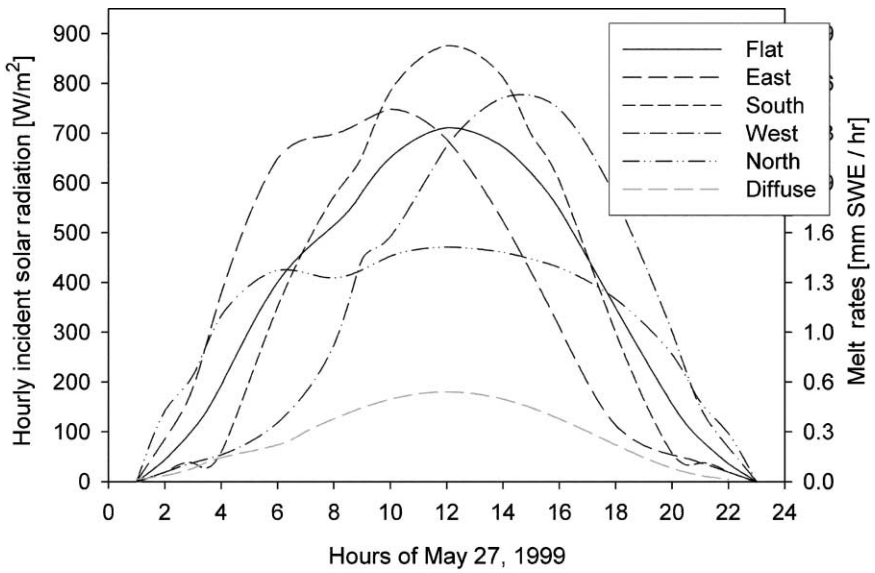

Figure 7 Incident solar radiation and resulting melt rates (assuming an albedo of 0.7) for hill slopes over 8° at different aspects and (theoretical) diffuse radiation for a completely cloudy day

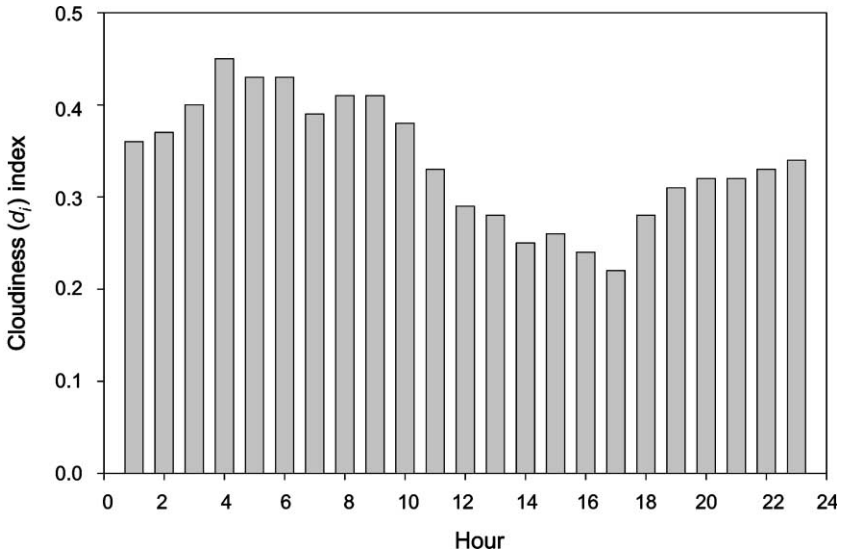

Figure 8 Average hourly cloudiness index (d_i) for three modelled spring periods

radiation was diffuse. The highest absolute values of incoming diffuse radiation were computed on partially cloudy days with cloudiness indices ranging from about 0.4 to 0.65. While increasing cloudiness increases both scattering and diffusion, thereby increasing the amount of diffuse radiation, clouds also reduce the overall quantity of incoming solar radiation by reducing the radiation amount available for scattering and diffusion (Granger and Gray 1990). As a result, snow covered basins have more evenly distributed melt rates on partially cloudy days. This may in effect lead to higher overall melt runoff volumes, compared to clear days, as potentially large shadowed areas (depending on the topography of the basin) contribute larger amounts of meltwater to runoff. Such an effect, however, could not be observed in this study due to the gentle relief of the study area.

The variability of total incident solar radiation was fairly constant for the three years, indicating that there is little inter-annual change in the spatial distribution of radiation due to topographic effects. Dubayah (1994) also found very similar variabilities for 4 years of

Table 2 Radiation model output statistics including cloudiness index d_i and % of incident diffuse solar radiation for three 11-d periods and the total modelling period (5 May–6 June) for three years of modelling

Date	Mean (MJ/m^2)	SD (MJ/m^2)	d_i (avg)	Diffuse (%)
5 May–15 May	191	3.3	0.33	50.0
16 May–26 May	216	3.3	0.33	49.2
27 May–6 June	227	3.1	0.36	51.6
5 May–6 June	634	9.7	0.34	50.2
5 May–15 May	202	3.5	0.28	45.1
16 May–26 May	227	2.9	0.29	45.5
27 May–6 June	225	2.9	0.37	52.2
5 May–6 June	654	9.2	0.32	47.6
5 May–15 May	209	4.1	0.25	42.1
16 May–26 May	224	3.0	0.30	46.3
27 May–6 June	241	3.2	0.31	46.7
5 May–6 June	673	10.2	0.28	45.1

modelling incident solar radiation in the much more rugged Rio Grande River basin. Intra-annually, the variability generally decreased slightly throughout the melt season due to increasing solar elevation angles.

Over the entire study period, the highest radiation values were located on steep south facing slopes (Figure 9(a)), while slopes with an easterly or westerly aspect received radiation amounts that were fairly close to the overall area wide mean. To better assess the importance of the obtained small-scale variabilities, amounts of potential snowmelt over the spring assuming a ripe snow cover were calculated. Net solar radiation was computed using a measured average (over the melt period) albedo of 0.65 for the snow cover. Areas within the entire model domain at opposite ends of the 2 standard deviation (SD) radiation range around the mean differ in their incident radiation amounts (over the entire model period) from 635 MJ/m^2 to 672 MJ/m^2 leading to a difference of 13 MJ/m^2 in net solar energy absorbed by the snow cover and therefore available for snowmelt. This would translate into a difference of 39 mm SWE for these locations. The differences are even greater within the study basin of TVC, where locations at opposite ends of the 2 SD range around the mean would differ in their potential melt by 53 mm SWE. One SD would still lead to a difference of 10 mm (13 mm within TVC). Considering that the average end-of-winter SWE for open tundra areas typically varies from about 50–120 mm SWE, these differences in potential melt have considerable implications for the development of a patchy snow cover as well as for the timing and volume of meltwater release.

Effect of changing scales

To assess the effects of changing resolutions on model results, the DEM was resampled at spacings of 120, 200 and 400 m. The resulting distributions of elevation and aspect remained virtually unchanged. However, there were large changes in slope values (Table 3), as mean and maximum slope as well as the standard deviation decreased considerably with decreasing resolution.

The model was run for the three additional grid resolutions for the spring of 1999. Hourly and overall area wide mean incident radiation was almost the same for all resolutions; however, the variability within the model domain decreased greatly (Table 4). Figures 9(a, b) show the accumulated spatially distributed values of incident solar radiation for two model scales (40 and 400 m). Figures 10(a, b) show the histograms illustrating the loss of information on spatial variability as model resolution increases. The effect of changing scales on snowmelt can be seen by comparing potential snowmelt values for locations at opposite ends of the 2 SD range around the mean for the different resolutions. The difference reduces from 39 mm for the 40 m resolution to 33 mm for 120 m, 28 mm for 200 m and 18 mm for 400 m.

Dubayah *et al.* (1990) show that the differences in spatial variability of incident solar radiation resulting from changing modelling scales should be linearly proportional to $\sin^2 SL$ within geographical regions, where SL is the average slope of the region dependent on the model resolution. The formula was derived from considerations of direct clear-sky radiation and theoretical constant terrain slope. Dubayah and van Katwijk (1992) demonstrated that the relationship also applies to incident solar radiation on real terrain for longer time periods with comparable average cloud conditions. The results shown in Table 4 indicate that the SD as a measure of variability calculated for the 3 additional DEM resolutions with this formula, agree well with those found from the simulations for our study area. This indicates that it might be possible to determine the effects of varying model scale on spatial variabilities from mean average basin slope for each DEM resolution after having run the complete model for at least one resolution. However, this approach does not provide any information on the

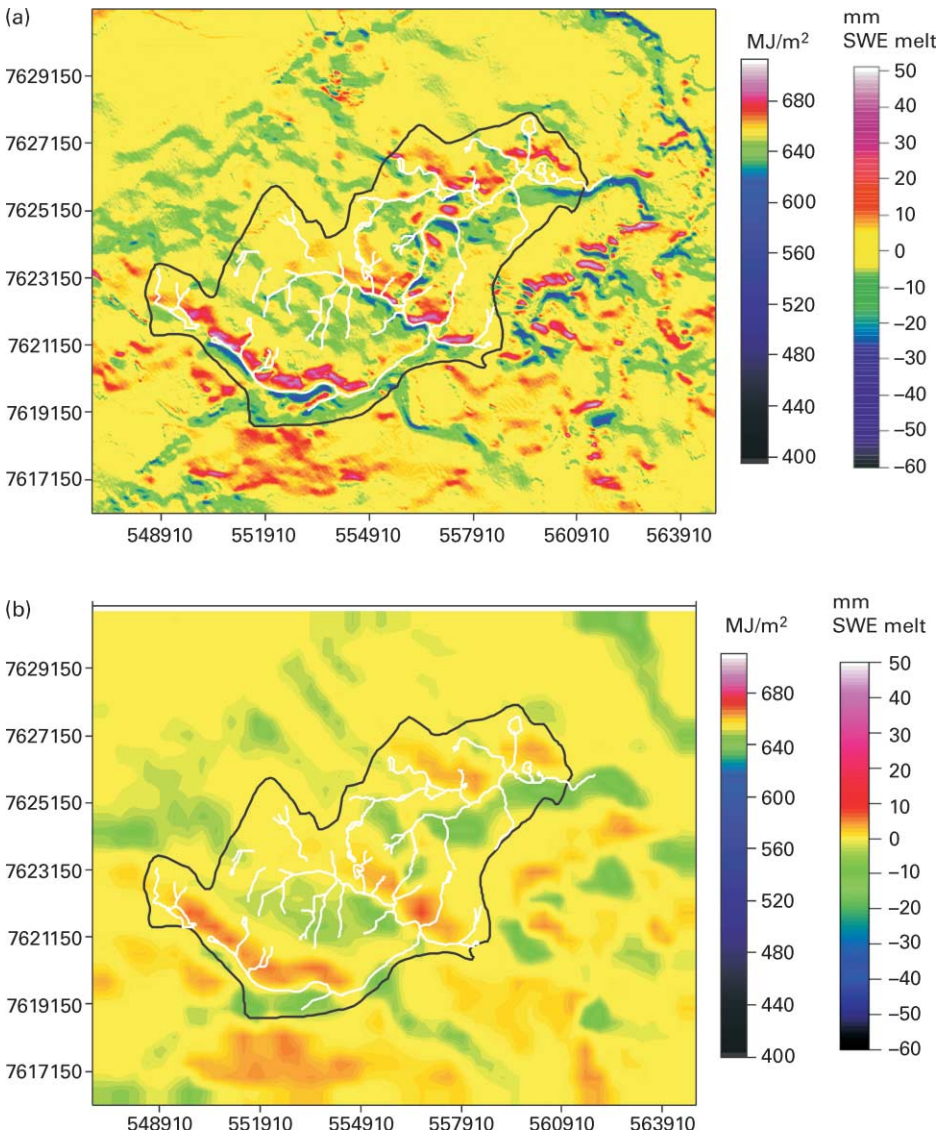

Figure 9 Spatially distributed incident solar radiation over entire model period 5 May to 6 June 1999 and resulting differences in potential snowmelt for (a) 40 × 40 m DEM and (b) for resampled DEM (400 × 400 m)

location of higher or lower than average energy fluxes within the model domain and the apparent shift of these locations with changing scales.

The results of the present study show that low radiation locations were greatly affected by changing model scales (Figures 9(a, b)). As grid sizes increased, the number of shadowed grid cells for a particular solar elevation angle decreased rapidly. Areas that are no longer

Table 3 Distribution of slopes in DEMs of different resolution

Resolution	40 m	120 m	200 m	400 m
Mean SL	2.6°	2.3°	2.1°	1.8°
Max. SL	32.2°	16.8°	12.9°	6.1°
SD of SL	2.5°	2.0°	1.6°	1.0°

Table 4 Statistics for total modelled spatially distributed incident solar radiation for 4 different resolutions for entire model period (33 d) ("Basin" values are measured data from the main meteorological station)

Resolution	Mean (MJ/m^2)	Range (MJ/m^2)	SD (MJ/m^2)	SD (% of mean)	SD (Dubayah equation) (MJ/m^2)
40 m	654	317	9.2	1.4	–
120 m	654	87	7.3	1.1	7.2
200 m	654	61	6.0	0.9	5.9
400 m	654	32	4.2	0.6	4.4
Basin	655	0	0	0	–

shadowed receive significant additional amounts of direct radiation and are therefore much closer to the average radiation values. In contrast, high radiation areas received less radiation with larger grid sizes due to reduced slope gradients. However, this effect was not as pronounced. A comparison of Figure 9(a, b) shows that a change in scale from 40–400 m greatly affects the location of extreme high and low radiation areas. Many of the highest accumulated radiation values for the 40 m spacings were located on short steep south facing slopes in TVC. These short slopes are not represented accurately at larger model scales, resulting in a shift of maximum radiation locations to parts of the basin characterized by longer but less steep slopes.

Absorbed and reflected radiation

The effects of varying model scale on simulated absorbed and reflected solar radiation, and therefore on overall surface radiation fluxes, were assessed for two days during the spring of

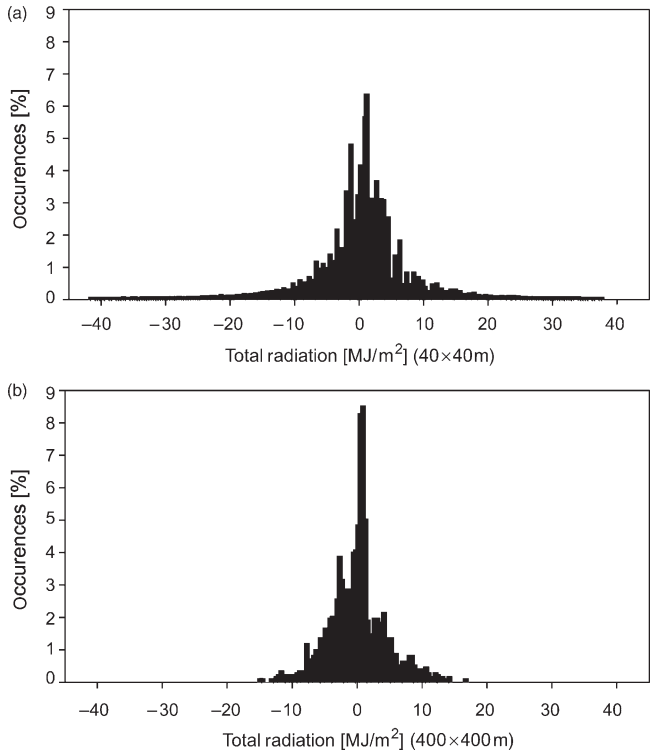

Figure 10 Histogram for total incident solar radiation as difference from the mean over entire model period 1999 for (a) 40 × 40 m DEM and (b) for resampled DEM (400 × 400 m)

1999 for which satellite images were available (23 May and 28 May). Grid cells were designated to be snow covered or snow free at a 10 m resolution and were assigned albedos of 0.7 and 0.2, respectively. The obtained spatially distributed albedo values were aggregated to match model resolutions and multiplied with daily distributed values of incident solar radiation from the model runs. Figure 11 shows the obtained map of absorbed solar radiation for 28 May for a resolution of 40 m. The map shows the extreme patchiness of the melting snow cover and the resulting large differences in the amount of absorbed short-wave radiation over short distances. Table 5 shows the mean and the standard deviation for the 4 different resolutions. Again, a greatly reduced variability can be observed for larger model resolutions, with the 400 m resolution showing a decrease in SD of about 43% compared to the 40 m resolution.

Discussion

Snowmelt is generally initiated at the top of a snow cover. As the meltwater percolates through the snowpack, two distinct wetting fronts are formed with a faster moving finger front advancing ahead of a background front (Marsh and Woo 1984; Marsh and Pomeroy 1996). The parts of a basin that contribute earliest to runoff are usually characterized by high melt rates and low end-of-winter snow depths. An example of such an area within TVC is shown in Figures 5(a–c) as box A. This location is close to the main channel and has steep west facing slopes. The dominant north-westerly winter winds of TVC typically lead to a lower than average end-of-winter snow cover for these slopes due to snow erosion during blowing snow events. This is combined with above average melt rates for westerly slopes due to higher than average late afternoon radiation (Figure 5(c)) coinciding with the late afternoon maximum of daily air temperatures (Hinzman *et al.* 1992). Consequently, the wetting fronts progress rapidly, quickly reaching the underlying ground surface and the area usually contributes to runoff earliest. Due to the proximity to the main channel, this location is often the first area where sufficient meltwater accumulates in the channel to initiate streamflow. If mean values of both snow depth and radiative melt energy were used, it would be difficult to explain this occurrence and to simulate the date of runoff initiation accurately.

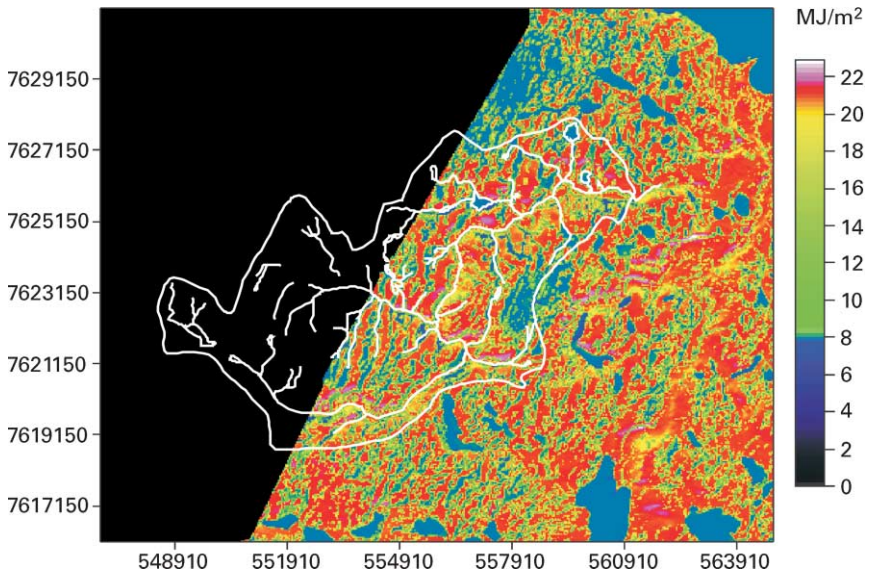

Figure 11 Absorbed solar radiation in MJ/m^2 for 28 May 1999. (Grid cells are 40 × 40 m). (No SPOT image was available for the blank area in the NW portion of the study area)

Table 5 Statistics of spatially distributed reflected and absorbed solar radiation for 4 different resolutions

	23 May				28 May			
Resolution	Mean absorbed (MJ/m^2)	SD (% of mean)	Mean reflected (MJ/m^2)	SD (% of mean)	Mean absorbed (MJ/m^2)	SD (% of mean)	Mean reflected (MJ/m^2)	SD (% of mean)
40 m	10.2	41.8	14.3	29.8	16.1	33.6	10.3	52.8
120 m	10.2	32.4	14.3	23.1	16.1	26.6	10.3	41.7
200 m	10.2	28.1	14.3	20.1	16.2	23.1	10.3	36.2
400 m	10.2	23.4	14.3	16.8	16.2	18.8	10.3	29.6

The spatial differences in incident radiation also affect runoff producing mechanisms. Once the ground has become bare large amounts of solar energy are absorbed, leading to the rapid development of a thawed layer at the top of frozen soils. This process proceeds more quickly in areas of above average solar radiation input as these areas tend to become bare earlier and continue to receive increased amounts of energy. A study by Quinton and Marsh (1999) showed that much of the hillslope runoff in arctic landscapes is generated through the upper peat layers. Hydraulic conductivities decrease rapidly as the thawed layer deepens and the water table recedes into less permeable soil layers. This means that areas of above average solar radiation contribute earlier to snowmelt runoff, but subsequently might become cut off from the hydrologic network sooner, as observed for south facing slopes by Carey and Woo (1999). It becomes evident that differences in solar radiation play an important role in determining the runoff producing areas of a basin, the quantities of meltwater released from these areas and the pace with which they reach the channel network. It is, therefore, important for hydrological snowmelt-runoff models to include a spatially variable solar radiation input, especially since many of these models are based on the principle of varying runoff source areas.

It would also be beneficial for such models to include a division of incident solar radiation into its direct and diffuse parts, as diffuse radiation determines the minimum amount of solar radiation available for warming and subsequent melting of the snowpack in all parts of the basin. In fact, it might be possible to create a simple, quasi-distributed, snowmelt energy model by first calculating or modelling diffuse and direct radiation amounts. Diffuse amounts could be applied evenly to entire basins, while time-dependent scaling factors could be used to distribute direct solar radiation on slopes of different steepness and aspect. The topography of the basin and the accuracy needed for the specific application would determine how many slope and aspect classes would have to be considered.

Land surface schemes (LSS), regional climate models and numerical weather prediction models often operate at scales that would treat the model area of this study ($18 \times 15\,km^2$) as a single grid box. It is, therefore, useful to look at how spatial distribution of solar radiation could be adequately represented in these models. The snow hydrology algorithms of some LSS treat individual grid boxes as either fully snow covered or completely bare. This assumption can lead to large errors in the surface energy balance during snowmelt in arctic catchments. This can be illustrated by an analysis of absorbed and reflected solar radiation for two days during the 1999 melt period. On 23 May, $10.2\,MJ/m^2$ of solar radiation were absorbed over the entire day by the surface while $14.3\,MJ/m^2$ were reflected back to the atmosphere (for a model resolution of 40 m). The snow covered area (SCA) for that day was 79% and the area would have been classified as snow covered by a LSS. Assuming an albedo of 0.7 the LSS would calculate values for absorbed and reflected solar radiation of $7.3\,MJ/m^2$ and $17.1\,MJ/m^2$, respectively, for 23 May. The SCA dropped to 39% for 28 May and,

consequently, the area would have been classified as snow free. Assuming an albedo of 0.2 for bare ground, modelled values for absorbed and reflected short wave radiation would have been computed to be 21.1 MJ/m^2 and 5.3 MJ/m^2, respectively, compared to 16.1 MJ/m^2 and 10.3 MJ/m^2 calculated from the small-scale analysis of this study (Table 5). These differences could have serious impacts on the model's ability to accurately simulate atmospheric processes. In fact, grid boxes in LSS are often around 25 km in resolution. The comparison of small scale (40 m) versus large scale (25 km) model results shows the considerable differences in absolute values of absorbed and reflected solar radiation over these grid squares. On 23 May, a large scale LSS would simulate a reflected solar radiation of 4.3×10^8 MJ or about 7×10^7 MJ more than the small scale simulation used in this study. Consequently, absorbed solar radiation would be under-predicted by a LSS by that amount. On 28 May, a LSS would assume the reflected solar radiation to be 1.25×10^8 MJ lower than in the small scale model simulation. This demonstrates that at the very least a sub-grid parameterization describing the approximate SCA for each individual grid box should be included in the LSS of atmospheric models.

Conclusions

A modelling approach is presented to simulate small-scale variabilities of incident solar radiation as a result of topography. A DEM and incoming global short-wave radiation data is needed to run the model. Modelled results of incoming global and diffuse short wave radiation agreed fairly well with point measurements made within the model domain.

The model was run for 33 d during the springs of 1998, 1999 and 2001 on an hourly basis from sunrise to sunset. Maximum variability was found for clear-sky days, especially during hours with low solar elevation angles in the morning and evening. An increasing cloud cover reduced variability throughout the model domain. Diffuse radiation amounts increased with increasing cloudiness up to cloudiness indices of about 0.65. Days with higher cloudiness indices showed higher relative but decreased absolute contributions of diffuse radiation. The study has shown that the calculation of incoming diffuse solar radiation amounts is important for studies of spatially variable snowmelt processes and should therefore be included as an output variable in climate models.

Accumulated small-scale variability in solar radiation for the entire melt period, along with the variable end-of-winter snowpack, were shown to be important factors for the development of a patchy snow cover, the timing and amount of meltwater release and the determination of runoff-contributing areas of a basin. The area wide mean values of distributed incident solar radiation were very close to observed measurements at the basin meteorological stations. However, distributing these measured values evenly over the model domain would result in considerable errors in the calculations of snowmelt rates and surface energy balance values for the steeper slopes of the basin. Over the model period differences of 38 MJ/m^2 in incident solar radiation resulting in 39 mm of potential snowmelt (assuming an albedo of 0.65) were simulated for these areas. These slopes play a crucial role for the hydrology and the surface energy balance of the area as they are the areas of first bare ground and late lying snowdrifts. This shows that small-scale spatial variability of incident solar radiation is a crucial factor for key hydrological, energetic and land surface atmosphere exchange processes, even in areas of relatively low relief.

The results of this study further illustrate that the small-scale spatial variability of solar radiation is an important issue in land–surface components of atmospheric models, including regional climate models, general circulation models and numerical weather prediction models. Since these models typically operate at grid sizes larger than the scale of land surface variability described in this study, it is necessary for these models

to parameterize the sub-grid variability of solar radiation, and other snowmelt related processes, in an efficient yet physically realistic way. This is especially crucial since land–surface schemes and macro-scale hydrological models are increasingly used in regional studies of snow cover variations and snowmelt simulations (Woo and Young 2004).

The overall spatial distribution of radiation within the model area did not show much inter-annual variability. This indicates that it might be possible to relate the variability of incident solar radiation over a study area to certain topographic terrain measures like mean slope and frequency distribution of slopes and aspects that are relatively easily available from DEM's or contour maps. The overall variability of radiation could then be predicted from measured or modelled point values of direct and diffuse radiation and certain key terrain measures. Further work in other basins with a variety of terrain types is needed to test this approach.

The model was run at four different scales ranging from a resolution of 40–400 m. The area wide means did not change much for the different scales while variability was reduced considerably at larger scales. The reduction in overall variability could be related to the change in average slope. The change in scale also affected radiation amounts and locations of below and above average radiation areas. Spatially distributed net short-wave radiation values were also greatly affected by the change in model scale.

Future studies should include the running of the model for different terrain types and different latitudes. Furthermore, the small-scale variability of other components of the snowmelt energy balance will need to be addressed in order to simulate the spatial distribution of snowmelt in arctic basins more accurately.

Acknowledgements

The authors would like to thank Cuyler Onclin, Natasha Neumann, Mark Russell, Ross MacKay and Steve McCartney for their essential help in collecting and interpreting field data. Field support was provided by the Aurora Research Institute. This study received funding and logistical support from NWRI, the Canadian GEWEX/MAGS program and the Polar Continental Shelf Project. The authors are grateful for the comments of two anonymous reviewers that greatly improved this manuscript.

References

Bloeschl, G., Kirnbauer, R. and Gutknecht, D. (1991). Distributed snowmelt simulations in an alpine catchment. 1. Model evaluation on the basis of snow cover patterns. *Wat. Res. Res.*, **27**, 3171–3179.

Brown-Mitic, C.M., MacPherson, I.J., Schuepp, P.H., Nagarajan, B., Yau, P.M.K. and Bales, R. (2001). Aircraft observations of surface-atmosphere exchange during and after snowmelt for different arctic environments: MAGS 1999. *Hydrol. Process.*, **15**, 3585–3602.

Brubaker, K., Rango, A. and Kustas, W. (1996). Incorporating radiation inputs into the Snowmelt Runoff Model. *Hydrol. Process.*, **10**, 1329–1343.

Carey, S.K. and Woo, M.K. (1999). Hydrology of two slopes in subarctic Yukon, Canada. *Hydrol. Process.*, **13**, 2549–2562.

Dana, G.L., Wharton, R.A., Jr and Dubayah, R. (1998). Solar radiation in the McMurdo Dry Valleys, Antartica. *Ecosystem Dynamics in a Polar Desert: The McMurdo Dry Valleys, Antarctica*, Antarctic Research Series, **72**, 39–64.

Dozier, J. (1978). A solar radiation model for a snow surface in mountainous terrain. *Proc., Modeling of Snow Cover Runoff*, US Army Cold Regions Research and Engineering Laboratory, Hanover, NH, pp. 144–152.

Dozier, J. (1980). A clear-sky spectral solar radiation model for snow covered mountainous terrain. *Wat. Res. Res.*, **16**, 709–718.

Dubayah, R. (1994). Modeling a solar radiation topoclimatology for the Rio Grande River Basin. *J. Veg. Sci.*, **5**, 627–640.

Dubayah, R. and van Katwijk, V. (1992). The topographic distribution of annual incoming solar radiation in the Rio Grande Basin. *Geophys. Res. Let.*, **19**, 2231–2234.

Dubayah, R. and Rich, P.M. (1995). A solar radiation model for GIS. *Int. J. Geogr. Inf. Syst.*, **9**, 405–419.
Dubayah, R., Dozier, J. and Davis, F.W. (1990). Topographic distribution of clear-sky radiation over the Konza prairie, Kansas. *Wat. Res. Res.*, **26**, 679–690.
Essery, R., Long, L. and Pomeroy, J.W. (1999). A distributed model of blowing snow over complex terrain. *Hydrol. Process.*, **13**, 2423–2438.
Granger, R.J. and Gray, D.M. (1990). A net radiation model for calculating daily snowmelt in open environments. *Nord. Hydrol.*, **21**, 217–234.
Hinzman, L.D., Wendler, G., Gleck, R.E. and Kane, D.L. (1992). Snowmelt at a small Alaskan Arctic watershed. 1. Energy related processes. *9th Int. Northern Research Basins Symposium, Saskatoon, SK, Canada. NHRI Symposium*, *No.* 10, pp. 171–197.
Iqbal, M. (1983). *An Introduction to Solar Radiation*, Academic Press, New York.
Male, D.H. and Granger, R.J. (1981). Snow surface energy exchange. *Wat. Res. Res.*, **17**, 609–627.
Marks, D., Domingo, J., Susong, D., Link, T. and Garen, D. (1999). A spatially distributed energy balance snowmelt model for application in mountain basins. *Hydrol. Process.*, **13**, 1935–1959.
Marsh, P. and Woo, M.K. (1984). Wetting front advance and freezing of meltwater within a snowcover 1. Observations in the Canadian Arctic. *Wat. Res. Res.*, **20**, 1853–1864.
Marsh, P. and Pomeroy, J.W. (1996). Meltwater fluxes at an arctic forest-tundra site. *Hydrol. Process.*, **10**, 1383–1400.
Marsh, P., Pomeroy, J.W. and Neumann, N. (1997). Sensible heat flux and local advection over a heterogeneous landscape at an Arctic tundra site during snowmelt. *Ann. Glaciol.*, **25**, 132–136.
Martin, E. and Lejeune, Y. (1998). Turbulent fluxes above the snow surface. *J. Glacial.*, **26**, pp. 179–183.
Munro, D.S. and Young, G.J. (1982). An operational net short-wave radiation model for glacier basins. *Wat. Res. Res.*, **18**, 220–230.
Neumann, N. and Marsh, P. (1998). Local advection of sensible heat in the snowmelt landscape of Arctic tundra. *Hydrol. Process.*, **12**, 1547–1560.
Obled, Ch. and Harder, H. (1978). A review of snowmelt in the mountain environment. In *Proc., Modeling of Snow Cover Runoff*, US Army Cold Regions Research and Engineering Laboratory, Hanover, NH, pp. 179–204.
Ohmura, A. (1982). Climate and energy balance on the arctic tundra. *J. Climatol.*, **2**, 65–84.
Pomeroy, J.W., Marsh, P. and Gray, D.M. (1997). Application of a distributed blowing snow model to the Arctic. *Hydrol. Process.*, **11**, 1451–1464.
Quinton, W.L. and Marsh, P. (1999). A conceptual framework for runoff generation in a permafrost environment. *Hydrol. Process.*, **13**, 2563–2581.
Ranzi, R. and Rosso, R. (1991). A physically based approach to modelling distributed snowmelt in a small alpine catchment. *Proc., Snow, Hydrology and Forests in High Alpine Areas*, Vienna, Austria, IAHS Publ., **205**, 141–150.
Ranzi, R. and Rosso, R. (1995). Distributed estimation of incoming direct solar radiation over a drainage basin. *J. Hydrol.*, **166**, 461–478.
Slater, A.G. *et al.* (2001). The representation of snow in land surface schemes: results from PILPS 2(d). *J. Hydrometeor.*, **2**, 7–25.
Soulis, E.D., Snelgrove, K.R., Kouwen, N., Seglenieks, F. and Verseghy, D.L. (2000). Towards closing the vertical water balance in Canadian atmospheric models: coupling of the land surface scheme CLASS with the distributed hydrological model WATFLOOD. *Atmos. Ocean*, **38**(1), 251–269.
Tian, Y.Q., Davies-Colley, R.J., Gong, P. and Thorrold, B.W. (2001). Estimating solar radiation on slopes of arbitrary aspect. *Agric. Forest Meteor.*, **109**, 67–74.
Woo, M.K. and Young, K.L. (2004). Modelling arctic snow distribution and melt at the 1-km grid scale. *Nord. Hydrol.*, **35**(4), 295–307.